Model-based Shape Analysis of Gas Concentration Gridmaps for Improved Gas Source Localisation

Achim Lilienthal, Felix Streichert, Andreas Zell
University of Tübingen, WSI
Sand 1, D-72076 Tübingen, Germany
{*lilien,streiche,zell*}*@informatik.uni-tuebingen.de*

***Abstract*— This work addresses the capability to use concentration gridmaps to locate a static gas source. In previous works it was found that depending on the shape of the mapped gas distribution (corresponding to different airflow conditions) the gas source location can be sometimes approximated with high accuracy by the maximum in the concentration map while this is not possible in other cases. This paper introduces a method to distinguish both cases by analysing the shape of the obtained concentration map in terms of a model of the time-averaged gas distribution known from physics. The parameters of the model that approximates the concentration map most closely are determined by nonlinear least squares fitting using evolution strategies (ES). The best fit also provides a better estimate of the gas source position in situations where the concentration maximum estimate fails. Different methods to select the most truthful estimate are introduced in this work and a comparison regarding their accuracy is presented, based on a total of 34h of concentration mapping experiments.**

Index Terms - Gas concentration mapping, gas source localisation.

I. Introduction

A major problem for gas source localisation in a natural environment is the strong influence of turbulence on the dispersal of gas. Turbulent transport is considerably faster than molecular diffusion [1]. Apart from very small distances where turbulence is not effective, molecular diffusion can thus be neglected concerning the spread of gas.

The second important transport mechanism for gases occurs due to prevailing fluid flows (advective transport). This mechanism is typically effective even in an indoor environment without ventilation due to the fact that weak air currents exist as a result of pressure (draught) and temperature inhomogeneities (convection flow) [2].

Turbulent flow comprises at any instant a high degree of vortical motion. Small scale eddies stretch and twist the gas distribution, resulting in a complicated patchy structure, which exhibits no smooth concentration gradients that indicate the direction toward the centre of a gas source [3]. Turbulence is chaotic in the sense that the instantaneous flow velocity at some instant of time is insufficient to predict the velocity a short time later. Consequently, a snapshot of the distribution of a target gas at a given instant contains little information about the distribution at another time. Assuming a uniform and steady flow, however, the *time-averaged* concentration field varies smoothly in space with moderate concentration gradients [1].

An algorithm to create gas concentration gridmaps that represent the time-averaged structure of a gas distribution from the gas sensor readings collected by a mobile robot was introduced by Lilienthal and Duckett [4]. The algorithm is summarised in Section III.

Gas concentration mapping is useful for any application that requires to estimate the average distribution of a certain gas. For example, mobile robots that are able to build such a map could provide valuable information in a rescue mission, or could be used in Precision Farming [5] to provide a non-intrusive way of assessing certain soil parameters or the status of plant growth to enable a more efficient usage of fertiliser.

This paper addresses the capability to use concentration gridmaps in order to locate a gas source. An obvious clue for the gas source position is the concentration maximum in the map. Experiments in an indoor environment indeed demonstrated that the concentration maximum estimate (CME) provides a satisfying approximation of the source location in many cases [6]. Under certain assumptions discussed in Section IV, gas spread due to a static, constantly evaporating gas source can be described on average as a Fickian diffusion process, ruled by a turbulent diffusion constant K (eddy diffusivity). Accordingly, it was observed that the distance between the CME and the true source location was small in case of a circular gas distribution. By contrast, the localisation capability of the CME was considerably degraded in cases where the concentration map showed a stretched out distribution, indicating a gas plume due to a dominant wind direction. According to the equations which describe the time-averaged stationary gas distribution (see Section IV), the concentration decreases slowly along the direction of a constant air current. Thus, even small inhomogeneities due to turbulence can cause a large displacement of the point of maximum concentration.

In this paper a method is presented that allows to distinguish situations, where the CME is a reliable approximation of the source location from situations where CME is unlikely to indicate the gas source position accurately. This is accomplished by comparing how well the concentration map can be approximated by a model known from physics

Fig. 1. Koala robot with the Örebro Mark III mobile nose and the gas source used in the experiments. The small image in the top left corner shows a Figaro gas sensor used in the Mark III mobile nose.

(see Section IV), which describes the time-averaged gas distribution under certain idealised assumptions.

Apart from providing a measure of the certainty of the CME, the introduced method allows to derive a better estimate of the gas source position in situations where the CME fails. To determine the model, which approximates the given concentration map most closely, the parameter set is optimised by means of nonlinear least squares fitting. Since the model parameters include the position of the gas source, the best fit naturally corresponds to an estimate of the true source position. In contrast to the CME, the best fit estimate (BFE) is derived from the whole distribution measured.

II. Experimental Setup

The experiments were performed with a Koala mobile robot equipped with the Mark III mobile nose [7], comprising 6 tin oxide gas sensors manufactured by Figaro (see Figure 1). This type of chemical sensor shows a decreasing resistance in the presence of reducing volatile chemicals in the surrounding air. Despite its drawbacks (low selectivity, comparatively high power consumption, weak durability, long response and recovery time), this type of gas sensor is most often used on mobile robots because it is inexpensive, highly sensitive and relatively unaffected by changing environmental conditions such as room temperature and humidity. The gas sensors were placed in sets of three (of type TGS 2600, TGS 2610 and TGS 2620) inside two separate tubes containing a suction fan each. Papst Fans (405F) were used to generate an airflow of 8 m^3/h. The distance between the two sets of sensors was 40 cm.

All experiments were performed in a rectangular laboratory room at Örebro University (size 10.6 $\times$ 4.5 m^2). The robot's movement was restricted so that its centre was always located inside the central region where precise and reliable position information is available from the external absolute positioning system W-CAPS [8], which was used to track the coloured cardboard "hat" on top of the robot (see Figure 1). The air conditioning system in the room was deactivated.

To emulate a typical task for an inspection robot, a gas source was chosen to imitate a leaking tank. This was realised by placing a paper cup filled with ethanol on a support in a bowl with a perimeter of 12 cm (see Fig. 1). The ethanol dripped through a hole in the cup into the bowl at a rate of approximately 50 ml/h. Ethanol was used because it is non-toxic and easily detectable by the tin oxide sensors.

III. Creating Gas Concentration Gridmaps

By contrast to metric gridmaps extracted from sonar or laser range scans, a single measurement from a gas sensor represents the measured quantity (the rate of redox reactions) only at the comparatively small area of the sensor's surface ($\approx$ 1 cm^2). Nevertheless, the gas sensor readings contain information about the average gas concentration of a larger area. First, this is due to the smoothness of the time-averaged gas distribution, which allows to extrapolate on the gas sensor measurements because the average gas concentration does not change drastically in the vicinity of the point of measurement. Second, the metal-oxide gas sensors perform temporal integration of successive readings implicitly due to their slow response and recovery time. The time constants of rise and decay for the complete gas sensitive system (mobile nose) used here were estimated as $\tau_r \approx 1.8$s and $\tau_d \approx 11.1$s respectively [7]. Thus spatial information is integrated along the path driven by the robot.

Based on these observations, the mapping technique introduced in [6] uses a Gaussian weighting function to model the decreasing likelihood that a particular reading represents the true average concentration with respect to the distance from the point of measurement. Each sensor reading is convolved using the radially symmetric two dimensional Gaussian function

$$f(\vec{x}) = \frac{1}{2\pi\sigma^2} e^{-\frac{\vec{x}^2}{2\sigma^2}}. \quad (1)$$

The weightings are calculated for each grid cell (i,j) by evaluating Eq. 1 at the distance $\vec{x} = \vec{x}^{(i,j)} - \vec{x}_t$ corresponding to the displacement of the centre of the grid cell $\vec{x}^{(i,j)}$ from the point $\vec{x}_t$ where the measurement was taken at time t. For each grid cell, the total sum of the weightings $W_t^{(i,j)}$ and the total sum of the weighted readings $WR_t^{(i,j)}$ are stored. A higher value of the sum of weightings corresponds to a higher density of concentration measurements in the vicinity of that particular grid cell. As a consequence, $W_t^{(i,j)}$ models the information content of a series of measurements in a way that assigns the strongest weight along the sensor trajectory. Here, the certainty about the average concentration is particularly high because the sensor readings represent a low-pass filtered concentration value integrated along the path driven, due to the memory effect of the metal oxide sensors.

Ultimately, if the sum of the weights $W_t^{(i,j)}$ exceeds a certain threshold value W_{min}, the grid cell is set to

$$c_t^{(i,j)} = WR_t^{(i,j)} / W_t^{(i,j)} \quad : \quad W_t^{(i,j)} \geq W_{min}, \tag{2}$$

representing an estimate of the relative concentration of a detected gas in that particular area of the environment. Otherwise the cell is considered unexplored.

In consequence of the memory effect of the gas sensors, the true average gas distribution appears distorted in the concentration map. As discussed in [6], however, this corruption is small. If the robot passes a given point from different directions, the mapping process results in a representation, which is broadened but not severely shifted compared to the real average concentration of a target gas. For the experiments considered in this work, this condition is fullfilled because either a predefined exploration path was used, where the path is passed equally often from opposite directions, or the robot was controlled as a gas-sensitive Braitenberg vehicle [9], and particular points were passed equally often from multiple directions on average. Thus, the mapping process results in a representation, which is broadened but not severely shifted compared to the real average concentration of a target gas.

While the actual value of the threshold W_{min} was found to have a minor influence on the resulting concentration map, the width σ of the Gaussian function is a critical parameter. Referring to the exploration path of the robot, it has to be chosen high enough to satisfy the requirement for sufficient extrapolation on the gas concentration measurements, but low enough to preserve the fine details of the mapped structures. In this paper, parameter values of $\sigma = 15$ cm, and $W_{min} = 10.0 \times$ (number of sensors) were chosen based on the considerations in [6].

Further details of the concentration mapping algorithm and a deeper discussion of the properties of concentration gridmaps especially regarding the slow response and recovery of the gas sensors are given in [6].

IV. Gas Distribution Model

Regarding the needs of mobile robotics, it is not feasible to model the turbulent wind and gas distribution in a realistic environment with the currently available technology. It is generally a problem that many boundary conditions are unknown. And even with a sufficiently accurate knowledge about the state of the environment it would be very time-consuming to achieve the required resolution with a conventional finite element model [10].

For specific situations the time-averaged distribution can be described in a computationally inexpensive way. Assuming isotropic and homogenous turbulence and a one-directional wind field with a possibly non-zero wind speed that is constant on average, the time-averaged gas distribution of a point source on the floor can be described as [11], [12]:

$$C(x,y) = \frac{q}{2\pi K}\frac{1}{r} e^{-\frac{V}{2K}(r - x_{\hat{w}})}, \tag{3}$$

$$r = \sqrt{(x_S - x)^2 + (y_S - y)^2}, \tag{4}$$

$$x_{\hat{w}} = \frac{\vec{x}\cdot\vec{w}}{|\vec{w}|} = (x_S - x)cos\theta + (y_S - y)sin\theta. \tag{5}$$

The concentration C at a point (x,y) level with the gas source is determined by the turbulent diffusion coefficient K, the location of the gas source (x_S, y_S), its release rate q, the wind speed V, and the upwind direction θ.

Eq. 3 comprises a term for symmetric $1/r$ decay and a second term that models asymmetric decay with respect to the wind direction. Since $x_{\hat{w}}$ is the projection of the displacement with respect to the source $\vec{x}$ to the upwind direction $\hat{w}$, the second term is constant along the upwind direction while the asymmetric decay is steepest in downwind direction.

The model introduced in Eq. 3 describes a system in the state of equilibrium where the gas source evaporates infinitely long into an infinite space. As a consequence, the model diverges at the source location, which is obviously an unrealistic description of the observed gas concentration. The symmetric term is replaced here by the spatial profile of the Green's function of the diffusion equation. For a fixed time (> 0) this function declines with $exp(-const \cdot r^2)$ and does not diverge at the source location. Consequently, the time-averaged gas distribution was modelled in this work as

$$\tilde{C}(x,y) = C_{00} e^{-C_S r^2} e^{-C_A(r - [(x_S - x)cos\theta + (y_S - y)sin\theta])} + C_B. \tag{6}$$

This model depends on seven parameters. C_{00} is the maximum concentration at the source location while C_S and C_A describe the magnitude of the symmetric and asymmetric decay, respectively. (x_S, y_S) are the coordinates of the point source and θ is the upwind direction, i.e. the angle between the upwind vector $\hat{w}$ and the x-axis. The parameter C_B is added in order to account for a non-zero base-level.

V. Model Selection

In order to compare a particular model with the observed concentration gridmap, the gas distribution predicted by the model is discretised to the gridmap. Then, the average deviation between the concentration value $c^{(i,j)}$ and the discretisised model value $\tilde{C}(x_i, y_j)$ predicted for the centre (x_i, y_j) of cell i, j is calculated over all explored cells as

$$\Delta = \sqrt{\frac{\sum_{i,j}(\tilde{C}(x_i, y_i) - c^{(i,j)})^2}{N}}, \tag{7}$$

with N being the total number of grid cells.

To search for the model that approximates a given concentration map most closely, in terms of minimising the sum in Eq. 7, an evolution strategy is applied. Evolution strategies (ES) are probabilistic, generational, population based search algorithms specialised on real-value optimisation problems. They have been developed by Rechenberg and Schwefel to solve practical optimisation problems in mechanical engineering [13], [14]. Instead of emphasising the analogy to

natural evolution, ES abstract the key elements of repeated selection and mutation, focussing on mutation rather than crossover. Often a self adapting mutation step size (also called strategy parameter) is used to increase the efficiency of the ES.

In this work, we use a (μ,λ)-ES with local mutation to solve the optimisation task. Each individual I stores seven model parameters p_k and seven strategy parameters σ_k for local mutation. Initially random individuals, i.e. models $\tilde{C}(x,y)$, are generated and their fitness is evaluated. Then, for each generation the μ best individuals are selected to generate λ new individuals through recombination of the model parameters p_k by crossover of two parents, followed by local mutation of the strategy and model parameters. Finally, the generational cycle of the ES is repeated with the offspring being the new population.

Local mutation enables independent adaptation of the strategy parameters for each dimension of the problem space by calculating the new strategy parameters σ'_k and the new model parameters p'_k as

$$\sigma'_k = \sigma_k \cdot e^{\tau \cdot N(0,1) + \tau' \cdot N_k(0,1)}, \tag{8}$$

$$p'_k = p_k + \delta p_k \cdot \sigma'_k \cdot N_k(0,1). \tag{9}$$

Here, δp_k is a range of values assigned to each parameter in advance, while $N(0,1)$ and $N_k(0,1)$ represent random numbers independently drawn from a normal Gaussian distribution. τ is an overall learning rate and τ' is a coordinate wise learning rate.

Based on several test runs where the model function was used with set parameters as the ground truth, the following parameters were chosen for this work: μ =10, λ =50, p_{mut} = 1.0 (mutation rate), p_{co} = 0.01 (crossover rate). The initial step width was set to $\sigma_k = \sigma_{init} = 0.1$. According to [15], the overall learning rate and the coordinate wise learning rate were chosen to be $\tau = 1/\sqrt{2\sqrt{n}} \approx 0.435$ and $\tau' = 1/\sqrt{2n} \approx 0.267$, respectively. The parameter ranges δp_k were chosen to be [0,5] for C_{00}, [0,20] for C_S and C_A, [-4,4] for x_0 and y_0, [-180°,180°] for θ, and [-1,1] for C_B. To avoid solutions corresponding to local rather than global minima of the fitness function in the search space, the whole fitting procedure was repeated four times while the ES was stopped each time after 25000 fitness calls. The best individual found was then selected and considered to be the best possible fit for the given concentration map.

VI. Sources of Inaccuracy

A perfect agreement between the obtained concentration gridmap and the model given by Eq. 6 cannot be expected in general for several reasons.

First of all, the assumptions the gas distribution model is based on might not be fulfilled. This mainly applies to the assumption of constant wind that does not change its direction during all the exploration. However, although no artificial air current was produced to create a dominant constant flow, the gas distribution was strikingly stable in the experiments presented in this paper and also in experiments in a similar indoor scenario, most likely due to stable temperature gradients in the room [2]. For that reason, the one-directional model can still be used to approximate the observed gas distribution. Expecting only minor deviations of the dominant air stream, the model will indicate the average wind direction while a poorer fitness value is expected in case of stronger changes of the wind direction.

A further assumption, which is not completely fulfilled, is that the concentration map represents the time-averaged gas distribution as it would appear over infinitely long time. Due to the local character of gas sensor measurements, it takes some time to build concentration gridmaps. In addition to spatial coverage, a certain amount of temporal averaging is also necessary to represent the time-constant profile of the gas distribution. The basic structures in the map were found to stabilise within the first hour of the mapping experiments [6], which were limited by the available battery capacity to approximately three hours of exploration. During this time transient concentration peaks caused by turbulence might not be sufficiently averaged out and thus can be preserved in the concentration map as minor deviations from the smooth course of the distribution. While this is generally more of a problem in regions of low concentration (because the peak to time-average ratio is higher there [1]), it is especially problematic if the robot is controlled as a gas-sensitive Braitenberg vehicle to avoid low concentrations, causing a low density of measurements in regions where the average concentration is low. The distortions due to rudiments of turbulent peaks tend to influence the fit result because the region of low concentration was typically much larger than the area of high concentration in the experiments considered in this work. In order to compensate for this effect, we use a modified fitness function that compares the square of the predicted value with the square of the normalised concentration value $\bar{c}^{(i,j)} \in [0,1]$.

$$\Delta = \sqrt{\frac{\sum_{i,j}(\tilde{C}^2(x_i,y_i) - \bar{c}^2_{i,j})^2}{N}}, \tag{10}$$

Hence, deviations in regions of low average concentration are reduced compared to deviations in regions of high average concentration before fitting.

The discussion in this section should have made clear that in addition to the obtained value of the fit parameters the fitness value itself has to be considered when analysing a concentration map as detailed in this paper. A poor fitness indicates that the applied model cannot describe the observed gas distribution faithfully, i.e. the model assumptions are not fulfilled. If so, the source position estimate obtained from the best fit cannot be considered reliable and the best information at hand is the CME. On the other hand, if a

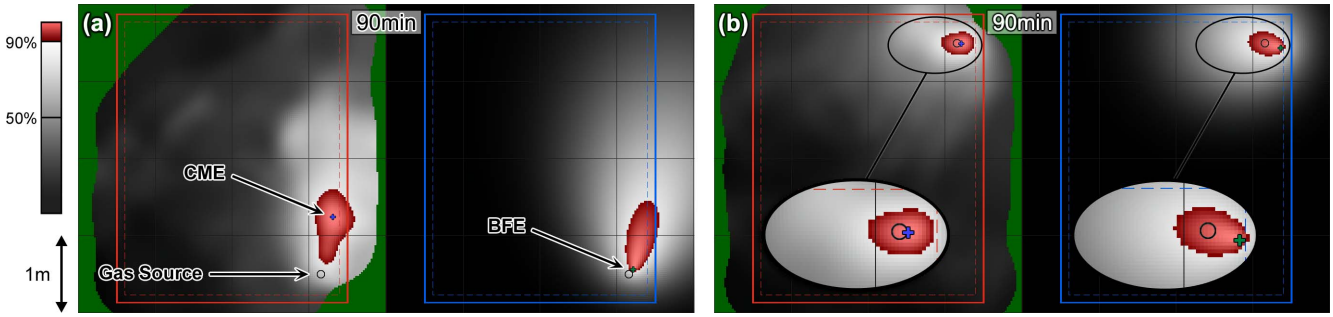

Fig. 2. Snapshots of concentration gridmaps (shown on the left side of both images) and the corresponding best fit result (right side). The concentration maps were created from data collected up to the time specified. Different shadings of grey are used to indicate concentration values (dark → low, light → high). Values higher than 90% of the maximum are displayed with a second range of dark-to-light shadings, and unexplored cells are visualised with another colour. Figure (b) contains a magnification of an elliptic area near to the source location, which is indicated in all images by a small circle. The two rectangles indicate the border region of the inspected area where a repulsive potential was used to keep the robot inside this virtual field.

good fitness can be achieved, the corresponding parameter set comprises a reasonable estimate of the source location as will be seen in the next section. Note that because of the difficulty to measure absolute concentrations with metal oxide gas sensors in an uncontrolled environment [3], the concentration map is created directly from the sensor readings. Although the calibration function of the gas sensors is nearly linear if a small range of concentrations is considered as in the experiments presented in this paper, it is therefore not possible to determine the absolute value of C_{00} and C_B. The remaining parameters, however, have a meaningful interpretation because they refer to the geometric dimension of the distribution profile. Therefore it is best to think of the method introduced in this paper as model-based *shape analysis* of gas concentration gridmaps.

VII. Results

Figure 2 shows snapshots of concentration gridmaps and the corresponding best fit result. The concentration maps were created from data collected up to the time specified in the figure during two different experiments where the robot was reactively controlled as a gas-sensitive Braitenberg vehicle. In both cases a good agreement between the observed concentration map and the best fit was obtained, indicated by a low fitness value. The fitting results, however, suggest that the experiments were carried out under different conditions. While the long stretched out shape of the fitted model displayed in Fig. 2,a points to a relatively strong air current, a weaker air stream is indicated by the more circular shape of the fit shown in Fig. 2,b. Such a difference is expressed by the ratio of the parameters C_A/C_B, which was 15.5 in case of the distribution in Fig. 2,a but only 2.8 for the distribution in Fig. 2,b. In case of a strong asymmetry, the CME is typically a poor approximation of the true source location. Due to the slow concentration decrease in upwind direction, small inhomogeneities of the wind field can cause a large displacement of the point of maximum concentration along the direction of the air current. As demonstrated by the example in Fig. 2,a the BFE is a more reliable estimate of the gas source position in case of a high ratio C_A/C_B.

On the other hand, the distance of the BFE to the gas source was often higher compared to the CME in case of a more symmetric distribution (see the example in Fig. 2,b). As mentioned in Section III, this is caused by the broadening effect due to the slow decay of the gas sensors. Regions of high concentration appear expanded in the map and consequently the fit results tend to be displaced with respect to the true gas source location by a certain amount. Here, the CME is a more accurate approximation of the gas source because the relatively steep descent of the average gas concentration prevents the observed maximum from being severely displaced by small deviations from the ideal distribution profile.

These observations suggest the following strategy for determining an improved estimate of the gas source location. The best matching fit is determined and the prediction error (fitness) and the C_A/C_S ratio are compared with corresponding threshold values t_f and $t_{A/S}$. If the obtained fitness is above t_f then the BFE is considered not reliable and the CME is used to estimate the source location. The CME is also chosen if a good fitness below t_f is obtained that indicates a relatively weak stationary air current. Finally, the BFE is used in case of a good fitness and a C_A/C_S value above $t_{A/S}$.

The accuracy of different gas source location estimates was compared based on 97 snapshots of concentration maps obtained in 11 mapping experiments, including a total of 34 hours of exploration. In four runs the robot moved along a predefined path (inwards and outwards a rectangular spiral) while it was reactively controlled as a gas-sensitive Braitenberg vehicle in the remaining seven trials. The explored area was approximately 2.4×2.4 m^2 in the experiments with a predefined exploration path, and it was approximately 3.75×3 m^2 in the Braitenberg vehicle experiments. Snapshots of the concentration map were taken in intervals of 15 minutes starting after one hour of exploration in order to refer to concentration maps, which represent mainly the stationary properties of the gas distribution (see Section VI).

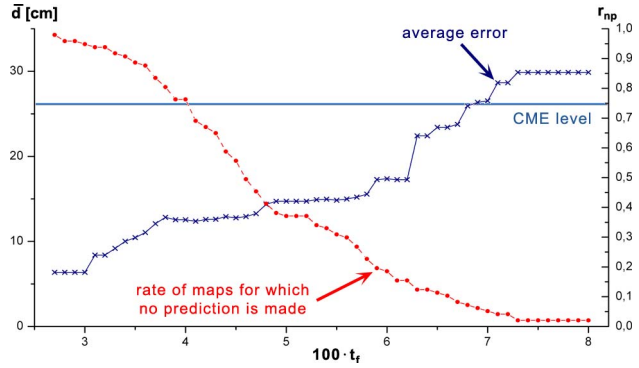

Fig. 3. Dependency of the average error of gas source prediction on the fitness threshold t_f if no prediction is made in case of a poor fitness of the best fit (crosses). The rate of concentration maps for which no prediction was made is also indicated (filled circles). The value of $t_{A/F}$ was set to 8.0.

A comparison of the results can be seen in Table I. The first column specifies when the BFE was chosen instead of the CME and the second column itemises the optimal threshold parameters required. Ultimately, the average distance between the estimate and the true source location is given in the third column. The obtained accuracy was 15% better compared to using only the CME if the BFE was always selected in case a good fitness, and it was 32% lower if the BFE was selected with the strategy introduced above that also considers the asymmetry of the fit result.

A further improvement of the accuracy can be obtained if it is acceptable to refuse a prediction of the source location in case both the BFE and the CME were found to be unreliable. The important observation in this context is that an unstable wind field, corresponding to a poor fitness value, causes an expanded region of high average concentration where the concentration maximum can vary due to rudiments of turbulent fluctuations in the concentration map. This entails an extended strategy that selects the BFE or the CME in case of a reliable best fit (depending on the asymmetry of the fit result) while it does not make a prediction in case of an unreliable best fit. The obtained accuracy and the percentage r_{np} of concentration maps where no prediction was made can be seen in Fig. 3, depending on the chosen fitness threshold t_f, and using a constant value of $t_{A/S}$ = 8.0. The graph also shows the level of accuracy of the CME.

Fig. 3 demonstrates that the obtained fitness is a suitable measure to evaluate the certainty of the gas source location estimate obtained from the CME or the BFE. Thus, it is either possible to derive an area around the estimate position where the source is expected with high certainty, or to choose a fitness threshold depending on the required accuracy.

strategy (when to choose BFE)	$t_f, t_{A/S}$	$\bar{d}$ [cm]
never	-, -	26.2 ± 20.9
if fitness $< t_f$	0.0470, -	22.2 ± 15.5
if fitness $< t_f$ and $C_A/C_S > t_{A/S}$	0.0575, 8.0	17.8 ± 10.4

TABLE I
ACCURACY OF DIFFERENT GAS SOURCE LOCATION ESTIMATES.

VIII. CONCLUSIONS

This work introduces a method for analysing concentration gridmaps based on fitting a model of the average gas concentration to the map. Two main benefits are provided by this analysis. First, it creates a possibility to interpret the mapped gas distribution by quantitative means, including the possibility to derive a certainty measure for approximating the source position with the concentration maximum estimate (CME), i.e. with the location of the maximal grid cell in the map. Second, the fit result provides also an estimate of the source location (best fit estimate, BFE), which was found to be more reliable than the CME if the mapping experiment was performed under conditions of a relatively strong constant air current, indicated by a high asymmetry of the best model found. These benefits were validated based on a total of 34h of mapping experiments, and a new estimate, which is obtained by selecting the BFE or the CME based on the quality of the best fit and ist asymmetry, was found to be 32% more accurate than the CME.

REFERENCES

[1] P. J. W. Roberts and D. R. Webster, "Turbulent Diffusion," in *Environmental Fluid Mechanics - Theories and Application*, K. T. John Steele, Steve Thorpe, Ed. Academic Press, 2002.

[2] M. R. Wandel, A. Lilienthal, T. Duckett, U. Weimar, and A. Zell, "Gas Distribution in Unventilated Indoor Environments Inspected by a Mobile Robot," in *Proc. of the IEEE Int. Conference on Advanced Robotics (ICAR 2003)*, Coimbra, Portugal, 2003, pp. 507–512.

[3] A. Lilienthal and T. Duckett, "Experimental Analysis of Gas-Sensitive Braitenberg Vehicles," *Advanced Robotics*, vol. 18, no. 8, pp. 817–834, December 2004.

[4] ——, "Creating Gas Concentration Gridmaps with a Mobile Robot," in *Proc. of the 2003 IEEE/RSJ Int. Conference on Intelligent Robots and Systems (IROS 2003)*, Las Vegas, USA, 2003, pp. 118–123.

[5] B. S. Blackmore and H. W. Griepentrog, "A Future View of Precision Farming," in *Proceedings of PreAgro Precision Agriculture Conference*, Müncheberg, Germany, Center for Agricultural Landscape and Land Use Research (ZALF), 2002, pp. 131–145.

[6] A. Lilienthal and T. Duckett, "Building Gas Concentration Gridmaps with a Mobile Robot," *Robotics and Autonomous Systems*, vol. 48, no. 1, pp. 3–16, August 2004.

[7] ——, "A Stereo Electronic Nose for a Mobile Inspection Robot," in *Proceedings of the IEEE International Workshop on Robotic Sensing (ROSE 2003)*, Örebro, Sweden, 2003, published in proceedings without page numbers.

[8] ——, "An Absolute Positioning System for 100 Euros," in *Proceedings of the IEEE International Workshop on Robotic Sensing (ROSE 2003)*, Örebro, Sweden, 2003, published in proceedings without page numbers.

[9] V. Braitenberg, *Vehicles: Experiments in Synthetic Psychology*. MIT Press/Bradford Books, 1984.

[10] G. Kowadlo and R. A. Russell, "Naive Physics for Effective Odour Localisation," in *Proceedings of the Australian Conference on Robotics and Automation*, 2003.

[11] H. Ishida, T. Nakamoto, and T. Moriizumi, "Remote Sensing of Gas/Odor Source Location and Concentration Distribution Using Mobile System," *Sensors and Actuators B*, vol. 49, pp. 52–57, 1998.

[12] J. O. Hinze, *Turbulence*. New York: McGraw-Hill, 1975.

[13] H.-P. Schwefel, *Numerical Optimization of Computer Models*. New York, NY, USA: John Wiley & Sons, Inc., 1981.

[14] I. Rechenberg, *Evolutionsstrategie: Optimierung technischer Systeme nach Prinzipien der biologischen Evolution*. Fromman-Holzboog, 1973.

[15] A. E. Eiben and J. E. Smith, *Introduction to Evolutionary Computing*. New York, NY, USA: Springer, 2003.